THESIS FOR THE DEGREE OF DOCTOR OF PHILOSOPHY IN SOLID AND
STRUCTURAL MECHANICS

Modelling crack-induced ultrasonic scattering in a thick-walled pipe

JACOB RUBENSON

Department of Applied Mechanics
CHALMERS UNIVERSITY OF TECHNOLOGY
Göteborg, Sweden 2017

Modelling crack-induced ultrasonic scattering in a thick-walled pipe
Thesis for the degree of Doctor of Philosophy in Solid and Structural Mechanics
JACOB RUBENSON
Department of Applied Mechanics
Chalmers University of Technology

ABSTRACT

Ultrasonic testing is used in several industries where there are high demands on safety, e.g. nuclear power and aerospace industries. In the nuclear industry and elsewhere there are many pipes that need to be tested. To this end this thesis considers ultrasonic wave scattering from a crack inside a thick-walled pipe. Several different crack types are considered: an infinite axial-radial crack, a finite axial-radial crack, and a radial-angular crack. To solve these problems a hypersingular integral equation method has been employed. The hypersingular integral equation is derived from an integral representation for the elastodynamic field that involves the Green's tensor of the pipe. The primary unknown in the integral equation is the crack opening displacement (COD). The Green's tensor of the pipe consists of two terms, one is the free space part, called the singular part, and an added part, called the regular part, to fulfil the stress free boundary conditions on the walls of the pipe. The regular part is derived in the first paper and is the same in all papers. The singular part for both the infinite and finite axial-radial cracks is a double Fourier representation in rectangular coordinates. The Green's tensor for the angular-radial crack is instead a Hankel transform representation. The hypersingular integral equation must be regularized and this is accomplished by expansions of the COD in Chebyshev functions, which have the correct square root behaviour along the crack edges. The integral equation also needs to be projected on the same set of Chebyshev functions, and this concludes the regularization. The COD can thereby be determined. The ultrasound in the pipe is excited by a probe on the outer wall of the pipe and a model for such a probe acting as transmitter is developed. The ultrasound from this probe act as the source term in the integral equation. As a receiver another probe is used and the action of this probe is modelled by a reciprocity argument where the output is the electric signal from the receiving probe. As a special and common case the same probe is acting as both transmitter and receiver, this is called pulse-echo testing. A few examples are given for the different crack types showing the influence of varying pipe diameter and wall thickness.

Keywords: Non-Destructive Testing, Cylindrical pipes, Hypersingular integral method, Ultrasonic waves, Crack

Acknowledgements

Thesis

This thesis consists of an extended summary and the following appended papers:

Paper A   J. Rubenson and A. Boström. Modelling of ultrasonic bulk wave scattering by an axial crack in a pipe. *Accepted* (2017)

Paper B   J. Rubenson, A. Boström, and P.-A. Jansson. Modelling of ultrasonic scattering by an axial-radial crack in a pipe. *Manuscript* (2017)

Paper C   J. Rubenson, A. Boström, and P.-A. Jansson. Modelling of ultrasonic scattering by an angular-radial crack in a pipe. *Manuscript* (2017)

The author of this thesis has performed most of the analytical calculations and the majority of the writing of the manuscripts in all papers. The code for paper A was mainly produced by the author of the thesis while the code for paper B and C was a joint effort with the co-authors. The analysis of the results has been in cooperation with the co-authors in all papers.

CONTENTS

Part I
Extended Summary

1 Introduction

1.1 Background

This thesis considers the mathematical modelling of non-destructive evaluation (NDE) and testing (NDT) of cracks in thick-walled pipes. According to Hellier [4] both NDE and NDT are common names for the technology to test objects without destroying it. It should be noted that there are more specializations than NDE and NDT, e.g. Quantitative Nondestructive Evaluation or QNDE, however, in this thesis there will be no distinction between NDE, NDT and QNDE. The application of NDE in this thesis will only be towards industry, however, there are other uses as well, e.g. medical ultrasound.

There are some structures where the structural integrity is paramount, e.g. nuclear power plants, oil pipelines and airplanes. These are the industries which can and do use NDE to ensure safety and functionality. There are many types of defects that can be found inside any metal structure and thus there exists many different methods of detecting these defects. The usage of NDE to continuously test for defects can increase longevity and safety for the structure and perhaps lower the maintenance cost for the industry.

There are several different types of defects; they can be located both inside (typically cracks), they can be located on the surface (typically erosions) and they can be surface breaking defects (typically cracks). The surface breaking defect is an obstruction that has either started as a submerged crack and propagated toward the surface or vice versa. The defects do not necessarily need to be empty, but can be filled with different materials ranging from other solids to fluids.

There are many techniques to perform NDT, many of these are described by Hellier [4] and some of these will be briefly mentioned here. Radiography is a technique which is similar to X-rays, a detector is placed behind the test object which is radiated. This method is used for welds and casts, however, there are limitations due to the thickness of the test object and to the fact that radiation is hazardous. Liquid penetrant is the utilization of dye to find surface breaking defects. Eddy current testing induces currents in the test subject and measures how the test object reacts to the current. If there is a defect present, a change in induced current can be measured, but this only works when the defect is very close to the surface.

Ultrasonic testing is usually performed by emitting a sound wave into the test object, usually with the frequency in the megahertz range, and recording the signal after the interaction with the defect. The test setup can be divided into pitch-catch, where the transmitter and receiver are on different locations, and pulse-echo where both the transmitter and receiver are on the same place. The pitch-catch method can use the distance between the transmitter and receiver is known and the time of flight can be used

to determine if a defect is present. The pulse-echo system records as the signal is sent and if there is an echo from a defect it can be recorded and interpreted. There are several books written on the subject, e.g. Langenberg et al. [5] and Hellier [4]. There are several possibilities to display the results, the most common ones are A-, B- or C-scans. The A-scan shows the signal strength as a function of time as the transducer is moved along the top of the test object. The B-scan is a side view scan that shows the depth of the defects using time of flight measurements. The C-scan is without the time dimension and can have both one or two spatial dimensions [4].

To model complex geometries often Finite Elements software or CIVA is used. CIVA is a software platform containing many different NDE modelling methods, including but not limited to ultrasound and radiography. CIVA is developed by the French government agency CEA[1]. The CIVA software uses a variety of approaches for the ultrasonic simulations, e.g. beam methods or FEA. The computational cost for purely numerical methods is often exhaustive and thus can impose limitations on the geometry. The solution is often to try to solve a 2D or simplified 3D version of the problem. There are also methods that employ a substantial analytical work before the computations on a computer begin, these are however limited to simple geometries but they can often be extended to 3D. Waterman [6] uses a matrix formulation called the T-matrix or null field approach. This method can be used to solve the scattering from several types of scatterers, some are given by Waterman [6]. Olsson [7] has used the T-matrix method to determine the scattered field from a spherical cavity inside a thick walled pipe.

There are also integral equation methods that can be applied to crack problems. These methods seem to have been introduced by Robertson [8], at least with the application towards elastodynamic problems. A type of integral equation method is the hypersingular integral equation method, this method has been used to model ultrasonic scattering, see Boström [9]. There are two different approaches to the hypersingular integral equation method, one that considers a Fourier transform of an unknown function and one that relates the Green's function to the scattered field. Boström [9] writes about the differences between the Green's function and Fourier transform methods and concludes that the Green's function method is more general. This can be shown by considering a crack in a layered medium, only the Green's function method can solve the problem if the crack and the layered medium are not aligned.

Considering the more specialized case of crack detection in pipes, most work has been done using guided wave finite element analysis. Ratasepp et al. [10] consider the interaction between the fundamental torsional mode and an axial crack in a pipe. The work by Demma et al. [11] considers different finite element models applied to crack detection in pipes. There is also research by Bai et al. [12] performed on a radial crack in pipe, however, they make approximations which allow them to solve two quasi-one dimensional equations instead of a three dimensional one. The research on cylindrical pipes using analytical methods is not as common as compared to half spaces or unbounded spaces. However, Olsson [7] has derived some interesting results on the reflection of ultrasonic waves inside a pipe.

---

[1]http://www-civa.cea.fr/en/

1.2 Purpose

The purpose of this thesis is to further the understanding of the wave propagation and scattering properties of different cracks inside a pipe. The behaviour of ultrasonic models in plates is well studied, for thick-walled pipes, however, this is not the case. Models for thick-walled pipes are needed to find out when the curvature of the pipe is important to consider. This knowledge would increase the efficiency of the modelling and more importantly, decide when it is a good approximation for the pipe to be approximated as a plate. It is also important to develop software that can be used to study examples of scattering inside pipes.

1.3 Limitations

This thesis is limited to cylindrical geometries, more specifically straight pipes. The work presented in the thesis is also limited to linear, homogeneous and isotropic material with complex Lamé parameters to simulate damping in the material.

2 Theory

2.1 Elastodynamics

Elastodynamic wave propagation is a well known phenomenon, several books have been written about this e.g. Graff [13], Achenbach [14] and Krautkrämer [15]. The elastodynamic equation of motion can be written is several different ways for a variety of different assumptions. This thesis will only consider linear wave motion inside in medium which is assumed to be isotropic and for a single frequency, ω. The equation of motion for the displacement field $\boldsymbol{u}$ can be written as (Graff [13], Achenbach [14])

$$k_p^{-2}\boldsymbol{\nabla}\boldsymbol{\nabla}\cdot\boldsymbol{u}(\boldsymbol{r}) - k_s^{-2}\boldsymbol{\nabla}\wedge\boldsymbol{\nabla}\wedge\boldsymbol{u}(\boldsymbol{r}) + \boldsymbol{u}(\boldsymbol{r}) = \boldsymbol{0}. \tag{2.1}$$

Here k_p and k_s are wave numbers and are defined accordingly $k_p^2 = \rho\omega^2/(2\mu + \lambda)$ and $k_s^2 = \rho\omega^2/\mu$. The subscript represent a pressure wave, k_p, or transverse wave, k_s. Here μ and λ are complex Lamé parameters and ρ is the density of the material. Throughout the thesis the factor $\exp(-\mathrm{i}\omega t)$ is omitted for brevity. The traction operator is defined as follows

$$\boldsymbol{t}^{(n)} = \hat{n}\lambda\boldsymbol{\nabla}\cdot\boldsymbol{u} + 2\mu\hat{n}\boldsymbol{\nabla}\boldsymbol{u} + \mu\hat{n}\wedge(\boldsymbol{\nabla}\wedge\boldsymbol{u}). \tag{2.2}$$

Depending on the geometry where the elastic waves propagate there are several possibilities to represent the solution. Boström et al. [16] have described several solutions in an unbounded geometry. In this thesis only the cylindrical basis functions will be discussed in detail and these are as follows,

$$\boldsymbol{\chi}_{1\sigma m}(\alpha;\boldsymbol{r}) = \sqrt{\frac{\epsilon_m}{8\pi}}\frac{1}{k_s\sin(\alpha)}\boldsymbol{\nabla}\wedge\left(\hat{z}\mathrm{H}_m(rk_s\sin(\alpha))e^{\mathrm{i}k_s\cos(\alpha)z}\begin{Bmatrix}\sin(m\varphi)\\\cos(m\varphi)\end{Bmatrix}\right),$$

$$\boldsymbol{\chi}_{2\sigma m}(\alpha;\boldsymbol{r}) = \sqrt{\frac{\epsilon_m}{8\pi}}\frac{1}{k_{s^2}\sin(\alpha)}\boldsymbol{\nabla}\wedge\boldsymbol{\nabla}\wedge\left(\hat{z}\mathrm{H}_m(rk_s\sin(\alpha))e^{\mathrm{i}k_s\cos(\alpha)z}\begin{Bmatrix}\sin(m\varphi)\\\cos(m\varphi)\end{Bmatrix}\right), \tag{2.3}$$

$$\boldsymbol{\chi}_{3\sigma m}(\alpha;\boldsymbol{r}) = \sqrt{\frac{\epsilon_m}{8\pi}\frac{k_p}{k_s^3}}\boldsymbol{\nabla}\left(\mathrm{H}_m(rk_p\sin(\alpha))e^{\mathrm{i}k_p\cos(\alpha)z}\begin{Bmatrix}\sin(m\varphi)\\\cos(m\varphi)\end{Bmatrix}\right).$$

Here, H_m is a Hankel function of the first kind and of order m, this set of basis functions represents outwards traveling waves. There are also regular waves ($\mathrm{Re}\boldsymbol{\chi}_{\tau\sigma m}$), which are obtained by replacing the Hankel functions with Bessel functions, J_m. The Neumann factor is defined as $\epsilon_m = 2 - \delta_{m0}$. The basis functions have several indices that represent the mode ($\tau = 1, 2, 3$), parity ($\sigma = o, e$) and order ($m = 0, 1, 2...$), which are combined to a multi-index, $\boldsymbol{\chi}_k \equiv \boldsymbol{\chi}_{\tau\sigma m}$. The first two modes are shear waves ($\tau = 1, 2$) and the third is a pressure wave ($\tau = 3$), the parity is determined by the parity of the trigonometric function. The complex parameter α belongs to $[0, \pi]$, C, C_-, C_+, the latter three curves can be seen in Fig. 2.1. Using these basis functions and the integral paths Green's tensors or vector representations for the displacement field can be created. The most common is if α is chosen to belong to C, this is a Fourier representation with the Fourier variable in the axial direction. The choice of C_- or C_+ will result in a Hankel transform representation,
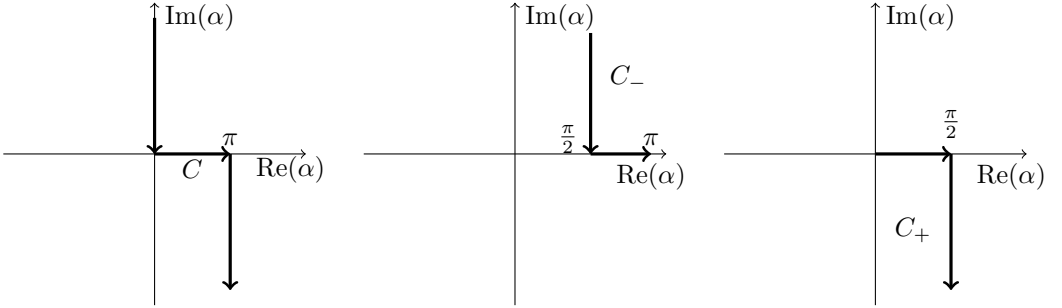
Figure 2.1: *The different integration paths for the complex parameter α.*

where the transform variable is in the radial direction. These will be used to construct the Green's tensor of the pipe and will be discussed later.

The basis functions in Eq. (2.3) cannot be used directly to solve for the scattered field from the crack since the geometry of the problem is not the same as for the free space problems. To mitigate this an alternative formulation can be is used, consider an infinite space with a scatterer present. This volume can be seen in Fig. 2.2, here both a scatterer with the volume V_s enclosed by a surface S_s and a transmitter with volume V_{in} enclosed by a surface S_{in} is inside a large spherical volume V which are enclosed by a surface S_R. The volume V becomes the entire space if the radius of the sphere approaches infinity, these situations have been investigated by Ström [17] and especially how to handle the boundary conditions at infinity. The integral representation is

$$-\frac{k_s}{\mu} \int_{S_R - S_{in} - S_s} \mathrm{d}S \left(\boldsymbol{u}(\boldsymbol{r}') \cdot \boldsymbol{t}^{(n)}(\mathcal{G}(\boldsymbol{r}, \boldsymbol{r}')) - \mathcal{G}(\boldsymbol{r}, \boldsymbol{r}') \cdot \boldsymbol{t}^{(n)}(\boldsymbol{u}(\boldsymbol{r}')) \right) = \begin{cases} 0, & \boldsymbol{r}' \notin (V) \\ \boldsymbol{u}(\boldsymbol{r}'), & \boldsymbol{r}' \in (V) \end{cases}$$

$$(2.4)$$

with the surfaces as shown in Fig. 2.2. Here $\mathcal{G}$ is the free space Green's tensor which satisfies the following equation

$$k_p^{-2} \boldsymbol{\nabla}\boldsymbol{\nabla} \cdot \mathcal{G}(\boldsymbol{r}, \boldsymbol{r}') - k_s^{-2} \boldsymbol{\nabla} \wedge (\boldsymbol{\nabla} \wedge \mathcal{G}(\boldsymbol{r}, \boldsymbol{r}')) + \mathcal{G}(\boldsymbol{r}, \boldsymbol{r}') = -k_s^{-3} \delta(\boldsymbol{r} - \boldsymbol{r}')\mathcal{I}, \qquad (2.5)$$

where $\mathcal{I}$ is the unit dyadic. The integral representation is derived by taking the difference between the equation of motion for the displacement field, Eq. (2.1), multiplied with the Green's tensor and the equation of motion for the Green's tensor, Eq. (2.5), multiplied with the displacement field and this difference is integrated over the volume $V - V_{in} - V_s$. The integral representation in its final form is found after using Gauss theorem. The details are omitted for brevity but are given by Ström [17].

There are many surfaces present in the present state of the integral representation, Ström [17] show that the contribution from the spherical surface integral becomes zero as the radius approaches infinity. In this thesis only passive scatterers are considered, and thus the displacement field can be divided into an incoming and a scattered field,

$$\boldsymbol{u} = \boldsymbol{u}^{\mathrm{in}} + \boldsymbol{u}^{\mathrm{sc}}. \qquad (2.6)$$
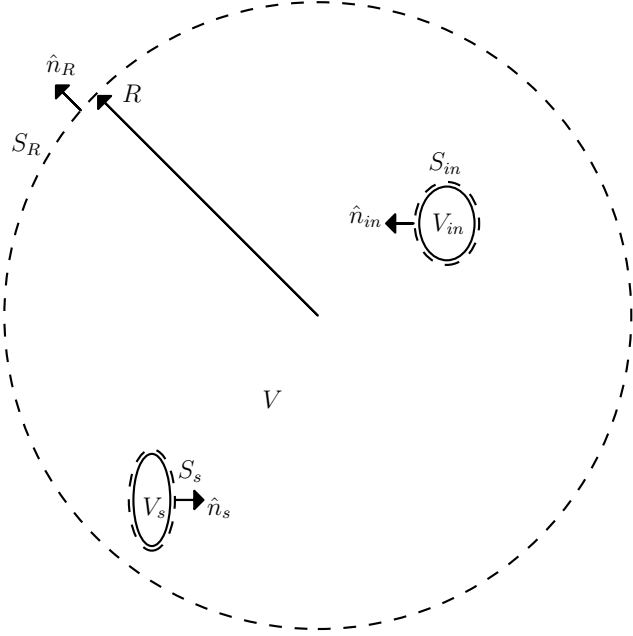
Figure 2.2: *The geometry for the integral representation.*

The integral representation can now be simplified to

$$
\boldsymbol{u}^{\mathrm{in}} + \frac{k_{\mathrm{s}}}{\mu} \int\limits_{S_{\mathrm{s}}} \mathrm{d}S \, \left(\boldsymbol{u}_+(\boldsymbol{r}') \cdot \boldsymbol{t}^{(\varphi)}(\mathcal{G}(\boldsymbol{r},\boldsymbol{r}')) - \mathcal{G}(\boldsymbol{r},\boldsymbol{r}') \cdot \boldsymbol{t}^{(\varphi)}(\boldsymbol{u}_+(\boldsymbol{r})) \right) = \begin{cases} 0, & r' \notin (V) \\ \boldsymbol{u}(\boldsymbol{r}'), & r' \in (V) \end{cases},
$$
(2.7)

where $\boldsymbol{u}_+$ is the displacement field evaluated in the limit on the surface S_s and $\boldsymbol{u}^{\mathrm{in}}$ is the incoming field from the volume V_{in} and is assumed to be known. This can be simplified even further if one only considers a crack surface, i.e. the volume has been collapsed to a surface. This also changes the displacement field $\boldsymbol{u}_+$ to $\Delta\boldsymbol{u}$ which is called the crack opening displacement (COD). The COD is the discontinuous jump in displacement over

the crack surface. The integral representation is now written as

$$\boldsymbol{u}^{\text{in}} + \frac{k_{\text{s}}}{\mu} \int\limits_{S_c} \mathrm{d}S\, \Delta\boldsymbol{u}(\boldsymbol{r}') \cdot \boldsymbol{t}^{(n)}(\mathcal{G}(\boldsymbol{r}, \boldsymbol{r}')) = \begin{cases} 0, & \boldsymbol{r}' \notin V, \\ \boldsymbol{u}(\boldsymbol{r}'), & \boldsymbol{r}' \in V. \end{cases} \tag{2.8}$$

One way to solve for the COD is to establish an integral equation.

2.2 Integral equations

To establish an integral equation the traction operator is applied to the integral representation, the boundary condition on the crack is used and the field point is taken on the crack surface to obtain the following

$$\boldsymbol{t}^{(n)}(\boldsymbol{u}^{\text{in}}(\boldsymbol{r}'))\Big|_{\boldsymbol{r}'=\boldsymbol{r}_{\text{o}}} = -\lim_{\boldsymbol{r}'\to\boldsymbol{r}_{\text{o}}} \frac{k_{\text{s}}}{\mu} \int\limits_{S_c} \mathrm{d}S'\, \Delta\boldsymbol{u}(\boldsymbol{r}') \cdot \boldsymbol{t}^{(n)}(\mathcal{G}(\boldsymbol{r}, \boldsymbol{r}')), \quad \boldsymbol{r}_{\text{o}} \in S_c. \tag{2.9}$$

It should be noted that $\boldsymbol{r}_{\text{o}}$ is not a constant but a parameterization such that the field point, $\boldsymbol{r}'$ is placed on the crack surface. However, the limit cannot be taken inside the integral when the traction operator has been applied. This is because the integral becomes hypersingular and cannot be evaluated in a proper sense. Martin and Rizzo [18] discuss hypersingular integrals and how to regularize them. The regularization process is depending on the shape of the crack, but generally it is about expanding the COD in functions that behave as the COD at the crack edges, where the COD goes as a square root.

2.3 A scalar example

The solution technique is quite complicated and as an illustrative example it is instructive to consider the similar 2D antiplane shear wave problem with a crack in a half plane. The boundary conditions on the boundary along the half plane and the tilted crack are stress free, i.e. the normal derivative is zero. The crack has a length $2a$, is tilted with the angle β counter clockwise and is placed in the upper half plane at the distance d to the boundary, as seen in Fig. 2.3. Two coordinate systems xy and $x_c y_c$ are introduced according to Fig. 2.3 and they are related as

$$x = x_c \cos(\beta) - y_c \sin(\beta), \tag{2.10}$$
$$y = d + x_c \sin(\beta) + y_c \cos(\beta), \tag{2.11}$$

where d is the distance between the crack and the half plane surface.

The displacement field has only a z component $\boldsymbol{u} = u(x, y)\hat{z}$ which satisfies Helmholz equation

$$\nabla^2 u + k^2 u = 0, \tag{2.12}$$
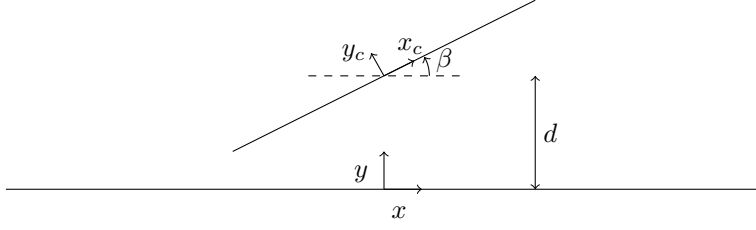
Figure 2.3: *The geometry of the half space with the crack.*

where k is the wave number. The Green's function for the half plane satisfies the same equation with a delta function on the right-hand side and can easily be expressed as

$$G(x, y; x', y') = \frac{i}{4\pi} \int_{-\infty}^{\infty} \frac{dq}{h} \left(e^{i|h(y-y')|} + e^{ih(y+y')} \right) e^{iq(x-x')}, \quad y' > 0 \qquad (2.13)$$

where $h = \sqrt{k^2 - q^2}$ with the chosen branch $\operatorname{Im} h \geq 0$. The first term in the Green's function is the singular part and the second term is the regular part which is added to satisfy the stress free boundary condition at $y = 0$. Inserting the coordinates into the Green's function, the final Green's function in the half plane becomes

$$G(x_c, y_c; x'_c, y'_c) = \frac{i}{4\pi} \int_{-\infty}^{\infty} \frac{dq}{h} \left(e^{i|h(y_c-y'_c)|} e^{iq(x_c-x'_c)} + \frac{1}{h} \exp[i(x_c(h\sin(\beta) + q\cos(\beta)) \right.$$
$$(2.14)$$

$$+ x'_c(h\sin(\beta) - q\cos(\beta)) + y_c(h\cos(\beta) + q\sin(\beta)) \qquad (2.15)$$

$$\left. + y'_c(h\cos(\beta) - q\sin(\beta)) + 2dh)] \right). \qquad (2.16)$$

The integral representation in this simple example becomes

$$u^{in}(x_c, y_c) + \frac{k}{\mu} \int_{S_c} dS' \Delta u(x'_c) \frac{\partial G(x_c, y_c; x'_c, y'_c)}{\partial y'_c} \bigg|_{y'_c=0} = \begin{cases} 0, & y' < 0 \\ u(x_c, y_c), & y' > 0 \end{cases}, \qquad (2.17)$$

where μ is the Lamé parameter. The integral representation has been simplified by the assumption that the traction on the crack surface is stress free. The next step is to apply the normal derivative to the integral representation and letting the field point approach the crack surface. This leads to the following

$$\frac{\partial u^{in}(x_c, y_c)}{\partial y_c} \bigg|_{y_c=0} = -\lim_{y_c \to 0} \frac{k}{\mu} \int_{S_c} dS' \Delta u(x'_c) \frac{\partial^2 G(x_c, y_c; x'_c, y'_c)}{\partial y_c \partial y'_c} \bigg|_{y'_c=0}, \qquad (2.18)$$

and when the normal derivative is applied for both the field and source points the field point cannot be taken inside the integral. The integral becomes hypersingular and must be regularized in some way. To do this the COD is expanded as follows

$$\Delta u = \sum_n \beta_n \psi_n(\frac{x'_c}{a}), \qquad (2.19)$$

where $\psi_n(s)$ are Chebyshev functions and β_n are the unknown expansion coefficients for the COD. The Chebyshev functions are a complete set of functions that form a basis and have the same square root behaviour at the crack edge as the COD. The Chebyshev functions can be defined as

$$\psi_n(s) = \begin{cases} \frac{-1}{m\pi}\cos(n\arcsin(s)), & n = 1, 3, \dots \\ \frac{\mathrm{i}}{m\pi}\sin(n\arcsin(s)), & n = 2, 4, \dots \end{cases} , \tag{2.20}$$

where s belongs to the interval $[-1, 1]$. These functions also have a very useful integral property

$$\int_{-1}^{1} \mathrm{d}s\, \psi_n(s)\mathrm{e}^{-\mathrm{i}\gamma s} = \frac{-1}{\gamma}\mathrm{J}_n(\gamma). \tag{2.21}$$

To finalize the regularization the integral equation needs to be projected on the same set of Chebyshev functions. The limit can now safely be taken inside the integral and after multiple usage of the integral property Eq. (2.21) the following system of equations can be established for the expansion coefficients

$$\sum_{n'} Q_{nn'}\beta_{n'} = T_n, \tag{2.22}$$

where

$$T_n = \int_{-a}^{a} \mathrm{d}x_c\, \psi_n(\frac{x_c}{a})\frac{\partial u^{\mathrm{in}}(x_c, y_c)}{\partial y_c}\Big|_{y_c=0}, \tag{2.23}$$

and

$$Q_{nn'} = nn' \int_{-\infty}^{\infty} \frac{\mathrm{d}q\, h}{q^2} \mathrm{J}_n(qa)\mathrm{J}_{n'}(qa) - nn' \int_{-\infty}^{\infty} \frac{\mathrm{d}q\, \mathrm{e}^{\mathrm{i}2dh}}{h}(h^2\cos^2(\beta) - q^2\sin^2(\beta)) \tag{2.24}$$

$$\times \frac{\mathrm{J}_n(a(q\cos(\beta) - h\sin(\beta)))}{q\cos(\beta) - h\sin(\beta)} \frac{\mathrm{J}_{n'}(a(q\cos(\beta) + h\sin(\beta)))}{q\cos(\beta) + h\sin(\beta)}. \tag{2.25}$$

Both these integrals are convergent, albeit the first one is only slowly convergent. However, this is a numerical problem that will be discussed in detail in the papers, but for the illustrative example it is enough to conclude that the expansion coefficients can be determined. Given that the expansion coefficients are known the COD is known and there are various ways of calculating either the scattered field u^{sc} or as in the articles the signal response.

3 Solution of the integral equation

In this section a brief overview of the appended papers is given. This shows the main differences between the papers and present some of the results. First the parts are given which are similar for all papers followed by a summary of the papers themselves. The section about the papers is very brief without the complicated mathematical manipulations, they can be found in the actual papers, however, the methodology is the same as for the illustrative example.

3.1 Green's tensors

The Green's tensor (function) is basically a tool to solve non-homogeneous partial differential equations [19]. The Green's tensor is the fundamental solution to the partial differential equation, however, in this thesis it is used in the integral representation. It should be noted here that in section 2.1 a pipe geometry is not considered. The integral representation for the pipe is derived in a very similar manner, but now the outer and inner surfaces of the pipe enter when applying Gauss' theorem to the elastic region (the pipe). Thus the basic integral representation is

$$-\frac{k_{\mathrm{s}}}{\mu} \int\limits_{S_+ + S_- - S_{\mathrm{in}} - S_{\mathrm{s}} - S_{\mathrm{p}}} \mathrm{d}S \left(\boldsymbol{u}(\boldsymbol{r}') \cdot \boldsymbol{t}^{(n)}(\mathcal{G}(\boldsymbol{r},\boldsymbol{r}')) - \mathcal{G}(\boldsymbol{r},\boldsymbol{r}') \cdot \boldsymbol{t}^{(n)}(\boldsymbol{u}(\boldsymbol{r}')) \right) \tag{3.1}$$

$$= \begin{cases} 0, & \boldsymbol{r}' \notin (V) \\ \boldsymbol{u}(\boldsymbol{r}'), & \boldsymbol{r}' \in (V) \end{cases} . \tag{3.2}$$

Here S_{p} is the pipe walls, S_{in} is the surface enclosing the sources, S_{s} is a surface enclosing the crack, and S_+ and S_- are surfaces far away making the pipe finite. As in section 2.1 the integral over S_{in} gives the incoming field and the integral over S_{s} introduces the COD. The integral over the walls of the cylinder vanishes when both the elastodynamic field and the Green's tensor satifiy traction free boundary conditions. The integrals over S_+ and S_- also vanish when the field and the Green's tensor are required to radiate energy outwards. The conclusion is that the integral representation and the integral equation are the same as for the generic case with a scatterer in full space considered in section 2.1, although it must remembered that the Green's tensor now is the one for the pipe and not the free space Green's tensor.

The Green's tensor for the pipe ($\mathcal{G}$) have a similar composition in all the papers, a singular part ($\mathcal{G}^{\mathrm{sing}}$) and a regular part ($\mathcal{G}^{\mathrm{reg}}$). The singular part is expanded in different ways depending on the crack, this is similar to using tilted coordinates that align with the crack as in the illustrative example. The singular part is a representation of the free space Green's tensor and in **Paper A** and **Paper B** the following form of the Green's tensor (Boström et al. [16]) is used

$$\mathcal{G}^{\mathrm{sing}}(\boldsymbol{r}';\boldsymbol{r}) = 2\mathrm{i} \sum_{j=1}^{3} \int_{-\infty}^{\infty} \int_{-\infty}^{\infty} \frac{\mathrm{d}q\,\mathrm{d}p}{k_j h_j} \boldsymbol{f}_j \boldsymbol{f}_j^* e^{\mathrm{i}(h_j|y'-y|+q(z'-z)+p(x'-x))}, \tag{3.3}$$

where the factors $\boldsymbol{f}_j$ and $\boldsymbol{f}_j^*$ are given in **Paper A** and **Paper B**. This is a double Fourier representation in rectangular coordinates transformed in x and z with the transform variables p and q, respectively. In **Paper C** the free space Green's tensor is a Hankel transform and it is

$$\mathcal{G}^{\text{sing}}(\boldsymbol{r}';\boldsymbol{r}) = 2\mathrm{i}\sum_k \int_0^\infty \mathrm{d}q\, \frac{q}{h_\tau} \mathrm{Re}\boldsymbol{\chi}_k(q;\boldsymbol{r})\mathrm{Re}\boldsymbol{\chi}_k^\dagger(q;\boldsymbol{r}'), \quad z > z'. \tag{3.4}$$

Here the cylinder functions from Eq. (2.3) are used and the integration curve is C_+ shown in Fig. 2.1. Thus $q = k_i \sin(\alpha) \in [0,\infty[$ and $h_i = \sqrt{k_i - q}$ $i = 1,2,3$, where $k_1 = k_2 = k_{\text{s}}$ and $k_3 = k_{\text{p}}$ is the shear wavenumber and 3 is the pressure wavenumber.

However, to create the Green's tensor for the pipe a so called regular Green's tensor is added. The added regular part is chosen in a manner that the sum of the regular and singular Green's tensors obeys traction free boundary conditions at both the inner and outer pipe surfaces. The determination of the regular part is based on the work of Olsson [7], who determined the reflection matrices for elastodynamic waves in a pipe. These reflection matrices where used in **Paper A** to determine the regular Green's tensor,

$$\begin{aligned}
&\mathcal{G}^{\text{reg}}(\boldsymbol{r}';\boldsymbol{r})\\
&= \mathrm{i}\sum_{kk'} \int_{-\infty}^\infty \frac{\mathrm{d}h}{k_\tau}\left(-\boldsymbol{\chi}_k(h;\boldsymbol{r})M_{kk'}^3(h)\boldsymbol{\chi}_{k'}^\dagger(h;\boldsymbol{r}') + \boldsymbol{\chi}_k(h;(r))M_{kk'}^4(h)\mathrm{Re}\boldsymbol{\chi}_{k'}^\dagger(h;\boldsymbol{r}')\right.\\
&\left.+\mathrm{Re}\boldsymbol{\chi}_k(h;(r))M_{kk'}^1(h)\boldsymbol{\chi}_{k'}^\dagger(h;\boldsymbol{r}') - \mathrm{Re}\boldsymbol{\chi}_k(h;(r))M_{kk'}^2(h)\mathrm{Re}\boldsymbol{\chi}_{k'}^\dagger(h;\boldsymbol{r}')\right) \tag{3.5}
\end{aligned}$$

Here $M_{kk'}^\nu$, $\nu = [1,2,3,4]$, are matrices that determine the reflections from a wave created by an arbitrary excitation. The number ν is related to geometrical reflection from the inner and outer surfaces of the pipe. These matrices are quite complex to calculate, but using a similar notation as Olsson [7] they can be written as follows

$$\boldsymbol{M}^1 = \boldsymbol{R}^{\text{o}}(\boldsymbol{I} - \boldsymbol{R}^{\text{i}}\boldsymbol{R}^{\text{o}})^{-1}\boldsymbol{R}^{\text{i}}, \tag{3.6}$$

$$\boldsymbol{M}^2 = \boldsymbol{R}^{\text{o}}(\boldsymbol{I} - \boldsymbol{R}^{\text{i}}\boldsymbol{R}^{\text{o}})^{-1}, \tag{3.7}$$

$$\boldsymbol{M}^3 = (\boldsymbol{I} - \boldsymbol{R}^{\text{o}}\boldsymbol{R}^{\text{i}})^{-1}\boldsymbol{R}^{\text{o}}, \tag{3.8}$$

$$\boldsymbol{M}^4 = (\boldsymbol{I} - \boldsymbol{R}^{\text{o}}\boldsymbol{R}^{\text{i}})^{-1}\boldsymbol{R}^{\text{i}}\boldsymbol{R}^{\text{o}}, \tag{3.9}$$

where $\boldsymbol{I}$ is the unit matrix. Here a short hand notation for matrix multiplication is used and the matrices $\boldsymbol{R}$ are reflection matrices which were derived by Olsson [7] and the superscript (i, o) represent inner or outer surfaces. The matrices are defined as

$$R_{kk'}^{\text{o}} = \sum_{k''} \mathrm{Re}S_{kk''}^{\text{o}}(h)(S^{\text{o}})_{k''k}^{-1}. \tag{3.10}$$

$$R_{kk'}^{\text{i}} = \sum_{k''} \mathrm{Re}S_{kk''}^{\text{i}}(h)(S^{\text{i}})_{k''k}^{-1}, \tag{3.11}$$

where $S_{kk'}^{\nu}$, $\nu = \mathrm{i}, \mathrm{o}$ are defined by

$$S_{kk'}^{\mathrm{i}} = \frac{k_{\mathrm{s}}}{\mu} \int_{S_{\mathrm{i}}} \mathrm{d}S \, \mathrm{Re}\boldsymbol{\chi}_k \cdot \boldsymbol{t}^{(r)}(\boldsymbol{\chi}_{k'}^{\dagger}), \tag{3.12}$$

$$S_{kk'}^{\mathrm{o}} = \frac{k_{\mathrm{s}}}{\mu} \int_{S_{\mathrm{o}}} \mathrm{d}S \, \mathrm{Re}\boldsymbol{\chi}_k \cdot \boldsymbol{t}^{(r)}(\boldsymbol{\chi}_{k'}^{\dagger}). \tag{3.13}$$

The $\mathrm{Re}S$ matrices are obtained by interchanging the basis function $\boldsymbol{\chi}_k$ to $\mathrm{Re}\boldsymbol{\chi}_k$ basis functions. The integrals in Eq. (3.12) can be performed analytically since the surfaces are circular cylinders. The analytically expressions for the matrices are calculated by Olsson [20]. It should be noted that the matrices $S_{kk'}$ and $\mathrm{Re}S_{kk'}$ are denoted $Q_{kk'}$ and $\mathrm{Re}Q_{kk'}$, respectively, by Olsson [20].

3.2 Complex Lamé parameters

The Lamé parameters in all the papers are complex. This is implemented by adding a small imaginary part to the Lamé parameters; $\mu = \mu^{\star}(1 - \mathrm{i}\epsilon)$ and $\lambda = \lambda^{\star}(1 - \mathrm{i}\epsilon)$. Here $\mu^{\star}$ and $\lambda^{\star}$ are the regular value of the Lamé parameters and ϵ is a small number that in all papers is 0.02 which corresponds to a realistic value. The usage of complex Lamé parameters simulate the damping inside the steel (mainly due to grain scattering) and it has the added benefit of increasing the numerical stability of certain integrals. The wave numbers become complex, with a positive imaginary part. The damping occurs when the wave numbers are complex as follows,

$$\exp(\mathrm{i}k_{\mathrm{s}}q) = \exp(\mathrm{i}qk_{\mathrm{s}}^{\star}(1 - \mathrm{i}\epsilon)^{-1/2}) \approx \exp(-.5qk_{\mathrm{s}}^{\star}\epsilon) \exp(\mathrm{i}qk_{\mathrm{s}}^{\star}). \tag{3.14}$$

Since ϵ is positive the first factor will have a damping effect. This is also the reason for the numerical stability for integrals over the integration variable q for large values of q.

3.3 Transmitting probe

The transmitting probe model is based on a model developed by Boström and Wirdelius [21] to model the incoming field from a planar surface. The model used here is modified to allow for the curvature of the pipe.

The incoming field, i.e. the field in the pipe in absence of the crack, is determined by solving the differential equation for elastic wave motion using the boundary condition stipulated by the probe model. The traction boundary condition is only nonzero in the normal direction on the outer pipe surface and is given as follows

$$t_r^{(r)}(\boldsymbol{u}) = \begin{cases} \mathrm{i}\mu k_{\mathrm{s}} \exp(-\mathrm{i}k_{\mathrm{s}}r_o \sin(\gamma)(\varphi - \varphi_0)), & \boldsymbol{r} \in S_1 \\ 0, & \boldsymbol{r} \notin S_1 \end{cases}. \tag{3.15}$$

Here S_1 is the surface where the probe is placed, and it can be described as

$$S_1 = \varphi \in [\varphi_0 - \delta, \varphi_0 + \delta], z \in [\zeta_0 - \zeta, \zeta_0 + \zeta]. \tag{3.16}$$
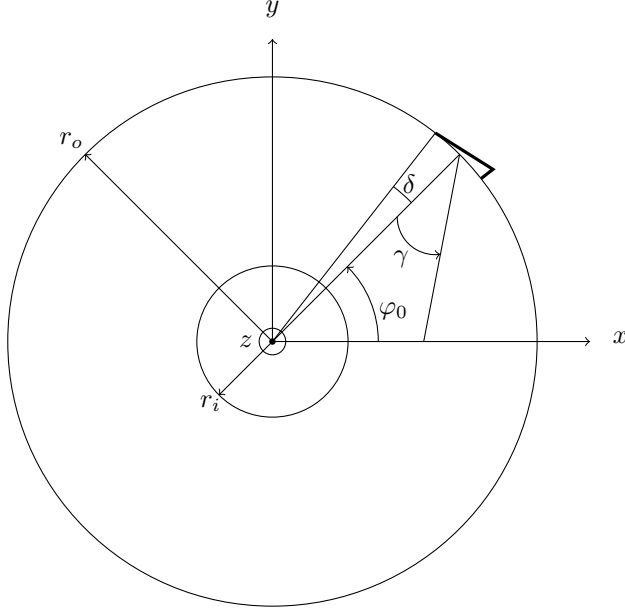
Figure 3.1: *The placement of the transmitting probe on the outer surface of the pipe.*

It should be noted that the probe is angled towards the normal using the angle γ, see Fig. 3.1. Here φ_0 and ζ_0 are the centre position for the probe in angular and axial directions and 2δ and 2ζ are the lengths of the probe in the angular and axial directions, respectively.

This boundary condition is only valid for **Paper A** and **Paper B**. To create the boundary condition for **Paper C** the probe needs to be angled towards the z axis, and thus a phase difference needs to be set on the axial direction instead. This is achieved by changing $(\varphi - \varphi_0)$ to $(z - z_0)$. The probe is a shear probe that is vertically polarized. However it is easy to change to a pressure probe by replacing the shear wave number (k_s) with the pressure wave number (k_p) in Eq. (3.15).

To obtain the field from the probe an eigenfunction expansion is used, the field is expressed using the following ansatz,

$$\boldsymbol{u}^{\text{in}} = \sum_k \int_{-\infty}^{\infty} \frac{\mathrm{d}h}{k_\tau} \left(\xi_k^1 \boldsymbol{\chi}_k + \xi_k^2 \text{Re} \boldsymbol{\chi}_k \right). \tag{3.17}$$

Here ξ_k^1 and ξ_k^2 are expansion coefficients that need to be determined from the boundary condition. The following equations can be set up for the unknown coefficients

$$\sum_k \int_{-\infty}^{\infty} \frac{\mathrm{d}h}{k_\tau} \left(\xi_k^1 \boldsymbol{t}^{(r)}(\boldsymbol{\chi}_k) + \xi_k^2 \boldsymbol{t}^{(r)}(\text{Re}\boldsymbol{\chi}_k) \right) = \hat{r} \mathrm{i} \mu k_s \exp(-\mathrm{i}k_s r_o \sin(\gamma)(\varphi - \varphi_0)), \quad r = r_o, \tag{3.18}$$

$$\sum_k \int_{-\infty}^{\infty} \frac{\mathrm{d}h}{k_\tau} \left(\xi_k^1 \boldsymbol{t}^{(r)}(\boldsymbol{\chi}_k) + \xi_k^2 \boldsymbol{t}^{(r)}(\text{Re}\boldsymbol{\chi}_k) \right) = 0, \quad r = r_i. \tag{3.19}$$

Expanding the right-hand side in trigonometric functions and a Fourier transform in the axial direction yields an equation system for the unknown coefficients that is be easily solved. These can be found in all papers and are not reproduced here.

3.4 Receiving probe

To obtain a signal from the crack a reciprocal theorem is used, this theorem and has been used in many similar applications, e.g. [22] and [9], and was developed by Auld [23]. The reciprocal theorem compares two different elastodynamic states and calculates the change in electric reflection coefficient between the states. The states are as follows; one with the defect and the transmitting probe present (state 1) and one without the defect but with the receiving probe acting as a transmitting probe (state 2). The change in electric reflection coefficient ($\delta\Gamma$) becomes more or less the quantity that is measured due to the effect of the defect. The reciprocal theorem is stated as follows

$$\delta\Gamma = \frac{\mathrm{i}\omega}{4P} \int_S \mathrm{d}S \left(\boldsymbol{u}_1 \cdot \boldsymbol{t}_2^{(n)} - \boldsymbol{u}_2 \cdot \boldsymbol{t}_1^{(n)} \right), \tag{3.20}$$

where the subscript shows the elastodynamic state, ω is the frequency of the incoming waves, P is the electric power exciting the transmitter, and n is the outward pointing normal on the surface S enclosing the defect.

Applying this to a crack surface, as considered in all papers, the boundary condition on the crack surface is traction free for the displacement field, $\boldsymbol{u}$. The signal response, Eq. (3.20) can thus be written as

$$\delta\Gamma = \frac{\mathrm{i}\omega}{4P} \int_{S_c} \mathrm{d}S \, \boldsymbol{\Delta u} \cdot \boldsymbol{t}^n(\boldsymbol{u}^{\mathrm{in}}). \tag{3.21}$$

Here the signal response ($\delta\Gamma$) can be calculated since in section 2.2 the COD ($\boldsymbol{\Delta u}$) is determined and in section 3.3 the incoming field ($\boldsymbol{u}^{\mathrm{in}}$) is determined. Comparing the differences between the papers it is noticed that in **Papers A** and **Paper B** the normal to the crack surface ($\hat{\varphi}$) is the same unlike **Paper C**, where the normal to the crack surface is $\hat{z}$ and also the surface itself is different between all papers.

3.5 Paper A

Paper A considers an infinite axial-radial crack in an infinitely long cylinder, see Fig. 3.2. The starting point is the hypersingular integral equation (2.8) with the singular Green's tensor in rectangular coordinates, Eq. (3.3) and the regular Green's tensor in cylindrical coordinates Eq. (3.5). To regularize the integral equation the COD is expanded as

$$\Delta u_n = \sum_{i=1}^{\infty} \int_{-\infty}^{\infty} \frac{\mathrm{d}p}{k_{\mathrm{s}}} \beta_{ni}(p)\psi_i \left(2\frac{r-a}{b-a} - 1 \right), \tag{3.22}$$

where $\beta_{ni}(p)$ are undetermined expansion coefficients depending on the axial Fourier transform variable p. The expansion in Chebyshev functions ψ_i, defined in Eq. (2.20), in
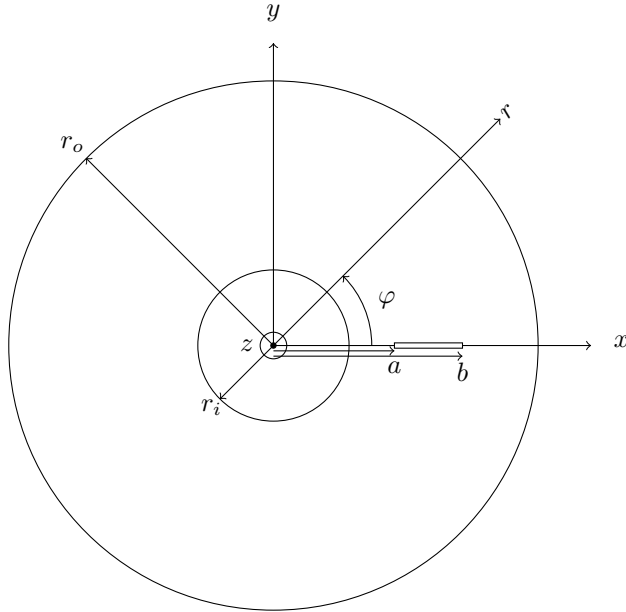
Figure 3.2: *The geometry of the pipe with the crack at $a \leq x \leq b$, In **Paper A** the crack is infinite in the axial direction, in **Paper B** it lies at $-d < z < d$.*

the radial direction is essential to regularize the hypersingularity in the integral equation. In the axial direction, where the crack is infinite, the expansion is a Fourier transform. Inserting the COD expansion into the integral equation, projecting the equation onto a Chebyshev function, and taking the Fourier transform of the equation gives a set of equations for the expansion coefficients with the Fourier transform variable p as a parameter. In the process the hypersingularity is regularized so the limit in front of the integral equation can be taken inside the integral. The transmitting and receiving probes are modelled as detailed above.

In the examples line scans in the angular direction is performed over the interval $0° < \varphi < 90°$ with a rectangular probe (10 mm by 10 mm) of shear wave type angled 45° and operating at the frequency 1 MHz. The pipe has outer radius 40, 50, or 60 mm and the wall thickness is 10 or 20 mm. The crack is 5 mm in width and starts 1 mm from the inner surface of the pipe. The material in the pipe is steel and the damping is $\epsilon = 0.01$.

The signal response as a function of probe position is shown in Figs. 3.3 and 3.4 showing the two different wall-thicknesses, respectively. In each figure results for all three pipe radii are shown. The results are shown in decibel and are normalized with the largest value in all the curves. The curves show the expected behaviour with peak values somewhere in the middle of the interval where the central ray from the probe hits the crack. The thicker pipe wall in Fig. 3.4 gives peak values for somewhat larger values of φ_0 which is also to be expected from ray considerations. The shear and pressure wavelengths are about 3 mm and 6 mm, respectively, so the wave propagation domain is not large in terms of wavelengths and this must be kept in mind when interpreting the results. With
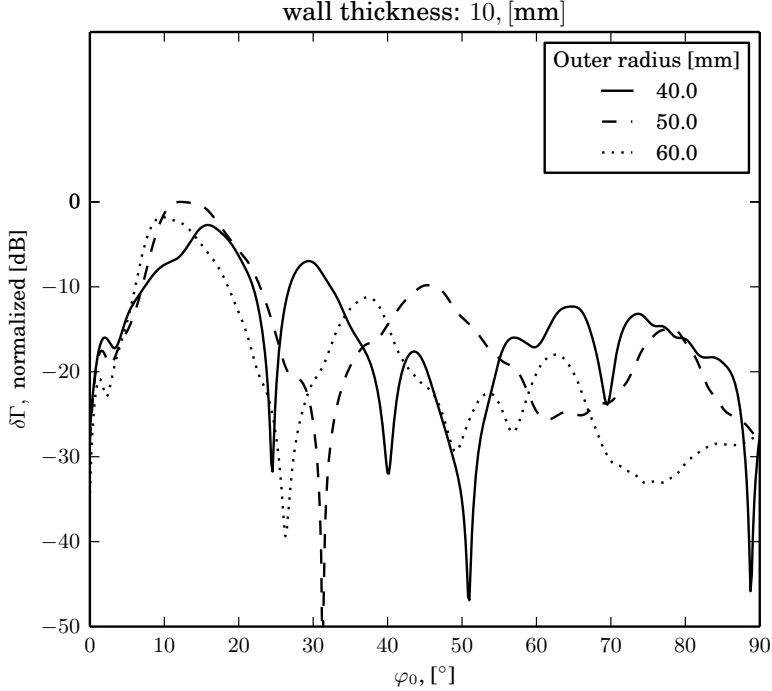
Figure 3.3: *Signal response as a function of the probe position, 45 ° probe, with the wall thickness is* 10 *mm and the crack is placed* 1 *mm from the inner surface*

increasing radii it is expected that the results should approach those for a plate. There is a tendency for the curves for the two larger radii 50 and 60 mm to be more close to each other than compared to the one for the smallest radius 40 mm. But the radii are still too small for the results to be comparable to those of a plate. Note in particular that the angle of the probe with the crack changes as the position of the probes changes.

3.6   Paper B

The crack in **Paper A** is infinite in the axial direction and this is only reasonable if the crack is at least a couple of wavelengths in the axial direction, and then it only models the signal response when all the waves from the probe hit the crack. It is of course of interest to also model a crack that is finite in the axial direction and this is done in **Paper B**, see 3.2 again. Much is then the same as in **Paper A**, the Green's tensor is expanded in the same way, but the COD is now expanded as

$$\Delta u_n = \sum_{i,j=1}^{\infty} \beta_{nij} \psi_i \left(2\frac{r-a}{b-a} - 1 \right) \psi_j \left(\frac{z}{d} \right) \tag{3.23}$$
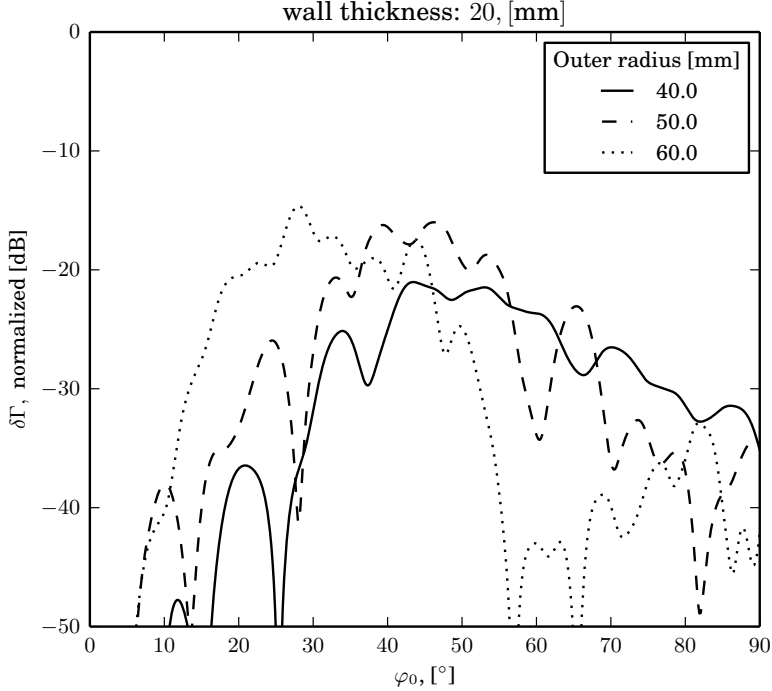
Figure 3.4: *Signal response as a function of the probe position,* $45\,^{\circ}$ *probe, with the wall thickness is* $20\,mm$ *and the crack is placed* $1\,mm$ *from the inner surface*

Here β_{nij} are the expansion coefficients and the Chebyshev functions are used as expansion basis in both coordinates. The projection of the hypersingular integral equation is then done on two Chebyshev functions, one for each coordinate, and the integral equation is hereby regularized. The transmitting and receiving probes are modelled as detailed above.

In Figs. 3.5 and 3.6 the signal response is shown as a function of φ_0. The pipe has a $60\,mm$ outer radius and a $10\,mm$ wall thickness. Three different z_0 values are compared $z_0 = 0\,mm$ (full-drawn curve), $z_0 = 2.5\,mm$ (dotted curve) and $z_0 = 5\,mm$ (dashed line). The z_0 values correspond to the center of the crack, half-way to the edge and at the edge, respectively.

In Fig. 3.5 the probe angle is $45\,^{\circ}$ and the largest peaks can be seen around $\varphi_0 = 15\,^{\circ}$ and as expected the highest peak is the one at the middle of the crack. The signal responds becomes weaker as z_0 becomes larger, as expected. As φ_0 is increased the signal response decreases, also as expected.

In Fig. 3.6 the probe angle is $30\,^{\circ}$ and the largest peaks can be seen around $\varphi_0 = 10\,^{\circ}$, and as expected the highest peak is the one at the middle of the crack, however, not by a lot. Compared to the results in **Paper A** similar trends are observed, i.e. the signal response becomes weaker as z_0 becomes larger. As φ_0 is increased the signal response decreases, however, not as fast as with the $45\,^{\circ}$ angled probe.
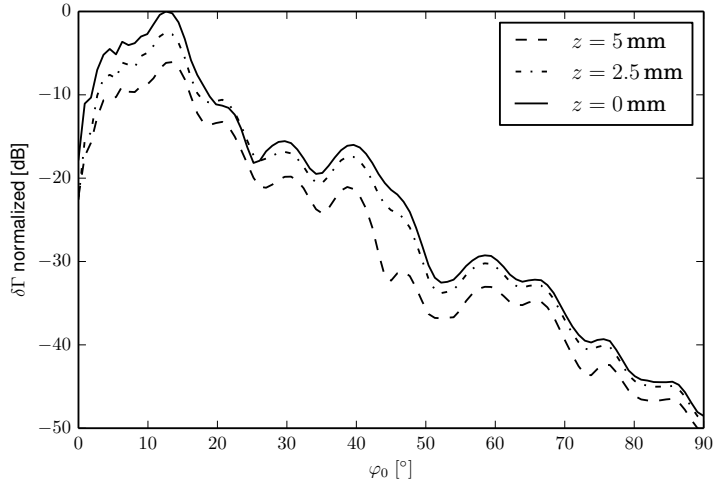
Figure 3.5: *Signal response as a function of the probe position, 45° probe, outer radius 60 mm, wall thickness 10 mm and the crack is placed 1 mm from the inner surface*
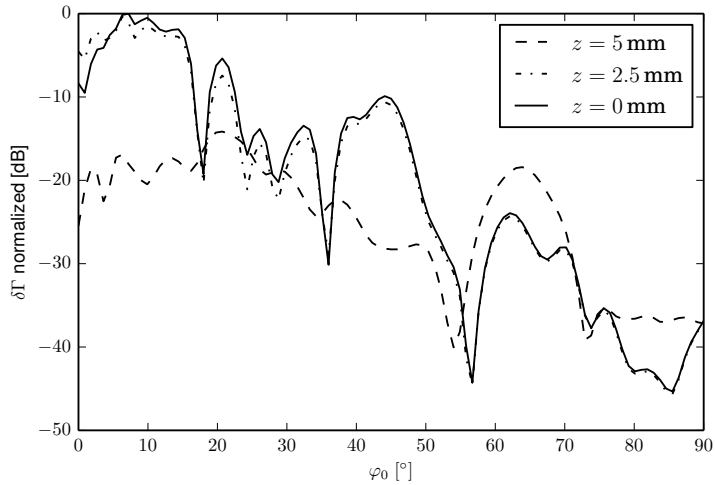
Figure 3.6: *Signal response as a function of the probe position, 30° probe, outer radius 60 mm, wall thickness 10 mm and the crack is placed 1 mm from the inner surface*
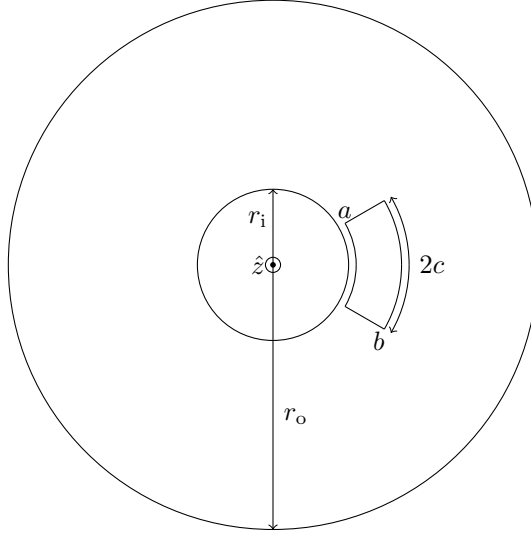
Figure 3.7: *The geometry of the pipe with the crack present.*

3.7 Paper C

In **Paper C** a different type of crack is considered, namely a finite angular-radial crack, see Fig. 3.7. The starting point is the hypersingular integral equation (2.8) with the singular Green's tensor in cylindrical coordinates, Eq. (3.4), and the regular Green's tensor in cylindrical coordinates, Eq. (3.5). To regularize the integral equation the COD is expanded as

$$\Delta u_n = \sum_{i,j=1}^{\infty} \beta_{nij} \psi_i \left(2\frac{r-a}{b-a} - 1 \right) \psi_j \left(\frac{\varphi}{d} \right) \tag{3.24}$$

Here β_{nij} are the expansion coefficients and the Chebyshev functions are used as expansion basis in both coordinates. The projection of the hypersingular integral equation is then done on two Chebyshev functions, one for each coordinate, and the integral equation is hereby regularized. As a technical detail it is noted that the asymptotic estimation of some integrals becomes a necessary ingredient to show that the regularization process has worked properly. The transmitting and receiving probes are modelled as detailed above.

In Fig. 3.8 the signal response is shown as a function of z_0 for two different angular probe positions, $\varphi_0 = 0\,°$ (full-drawn curve) and $\varphi_0 = 15\,°$ (dashed curve). These can be compared to the angular width of the crack $c = 30\,°$. In Fig. 3.8 z_0 is varied between -5 and $10\,\text{mm}$ and as the probe is moved over the crack, $z_0 < 0$, the signal response decreases rapidly, and as $z_0 > 0$ increases height of the peaks decreases slowly.

In Fig. 3.9 the signal response is shown as function of φ_0 for a fixed $z_0 = 2.5\,\text{mm}$. As the previous results have shown (Fig. 3.8) the signal response decreases dramatically as the probe approaches the crack edge.
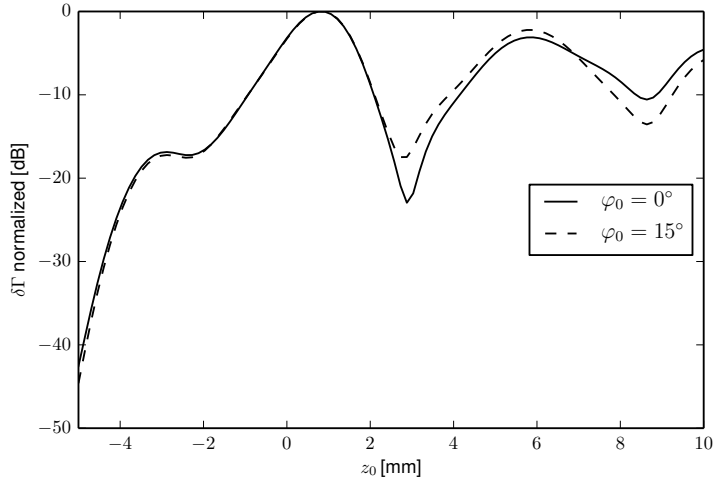
Figure 3.8: *Signal response as a function of the probe position, 45 ° probe, outer radius 40 mm, wall thickness 10 mm and the crack is placed 1 mm from the inner surface*
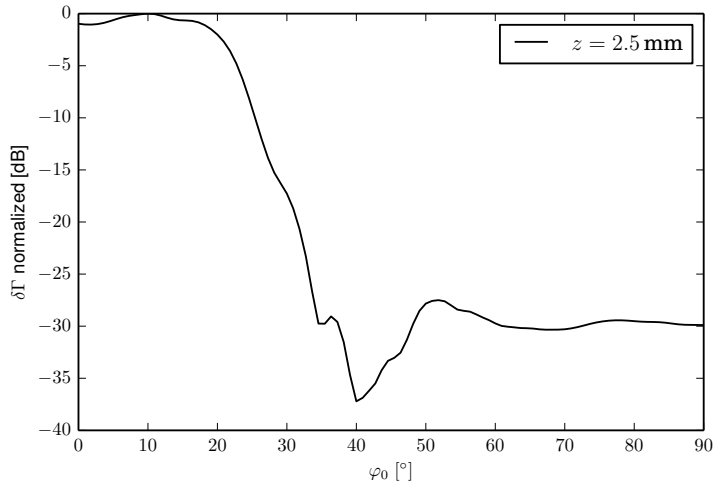
Figure 3.9: *Signal response as a function of the probe position, 45 ° probe, outer radius 40 mm, wall thickness 10 mm and the crack is placed 1 mm from the inner surface*

4 Final words

4.1 Conclusion

This work shows how the hypersingular integral equation method can be applied to several different types of cracks in a cylindrical pipe. The work also includes realistic models of ultrasonic probes acting as both transmitters and receivers. Some numerical examples are given, but it is desirable to perform further parametric studies. It is also very useful to compute time domain results and this can be done straightforwardly by a running a number of frequencies and perform a Fourier transform. This kind of studies may also be used to help create a database with responses when solving inverse problems or when calculating probability of detection curves.

4.2 Future work

There are several possibilities to extend the present work, one important case is to allow for surface breaking cracks. To do this the expansion in Chebyshev functions must be changed as the condition at the crack mouth is changed. It is also of interest to consider more advanced transmitting probes, such as phased array probes. More complicated cracks can also be considered, for example a rectangular crack that is tilted in an arbitrary way.

References

[1] J. Rubenson and A. Boström. Modelling of ultrasonic bulk wave scattering by an axial crack in a pipe. *Accepted* (2017).

[2] J. Rubenson, A. Boström, and P.-A. Jansson. Modelling of ultrasonic scattering by an axial-radial crack in a pipe. *Manuscript* (2017).

[3] J. Rubenson, A. Boström, and P.-A. Jansson. Modelling of ultrasonic scattering by an angular-radial crack in a pipe. *Manuscript* (2017).

[4] C. Hellier. *Handbook of Nondestructive Evaluation, Second Edition.* New York: McGraw-Hill, 2012. ISBN: 9780071777148.

[5] K.-J. Langenberg, R. Marklein, and K. Mayer. *Ultrasonic nondestructive testing of materials: theoretical foundations.* Florida: CRC press, 2012. ISBN: 978-1-4398-5588-1.

[6] P. C. Waterman. Matrix theory of elastic wave scattering. *J. Acoust. Soc. Am.* **60**.3 (1976), 567–580. DOI: 10.1121/1.381130.

[7] S. Olsson. Point force excitation of a thick-walled elastic infinite pipe with an embedded inhomogeneity. *J. Engng. Math.* **28**.4 (1994), 311–325. DOI: 10.1007/BF00128750.

[8] I. A. Robertson. Diffraction of a plane longitudinal wave by a penny-shaped crack. *Math. Proc. Cambridge Phil. Soc.* **63**.01 (1967), 229–238.

[9] A. Boström. Review of hypersingular integral equation method for crack scattering and application to modeling of ultrasonic nondestructive evaluation. *App. Mech. Rev.* **56**.4 (2003), 383–405.

[10] M. Ratassepp, S. Fletcher, and M. J. S. Lowe. Scattering of the fundamental torsional mode at an axial crack in a pipe. *J. Acoust. Soc. Am.* **127**.2 (2010), 730–740. DOI: 10.1121/1.3277185.

[11] A. Demma, P. Cawley, M. J. S. Lowe, and A. G. Roosenbrand. The reflection of the fundamental torsional mode from cracks and notches in pipes. *J. Acoust. Soc. Am.* **114**.2 (2003), 611–625. DOI: 10.1121/1.1582439.

[12] H. Bai, A. Shah, N. Popplewell, and S. Datta. Scattering of guided waves by circumferential cracks in composite cylinders. *Int. J. Solids Struct.* **39**.17 (2002), 4583–4603. DOI: 10.1016/S0020-7683(02)00339-6.

[13] K. F. Graff. *Wave Motion in Elastic Solids.* Dover Publications, 1991. ISBN: 0486667456.

[14] J. D. Achenbach. *Wave propagation in elastic solids.* New York: North-Holland, 1973. ISBN: 0444104658.

[15] J. Krautkrämer and H. Krautkrämer. *Ultrasonic testing of materials.* Berlin: Springer, 1983. ISBN: 9783540117339.

[16] A. Boström, G. Kristensson, and S. Ström. "Transformation properties of plane, spherical and cylindrical scalar and vector wave functions". *Field Representations and Introduction to Scattering.* Ed. by V. V. Varadan, A. Lakhtakia, and V. K. Varadan. Amsterdam: Elsevier, 2000, pp. 165–209.

[17] S. Ström. "Introduction to integral representations and integral equations for time-harmonic acoustic, electromagnetic and elastodynamic wave fields". *Field*

Representations and Introduction to Scattering. Ed. by V. V. Varadan, A. Lakhtakia, and V. K. Varadan. Amsterdam: Elsevier, 2000, pp. 37–143.

[18] P. A. Martin and F. J. Rizzo. Hypersingular integrals: how smooth must the density be? *Int. J. Numer. Methods Eng.* **39**.4 (1996), 687–704. DOI: `10.1002/(SICI)100207(19960229)39:4<687::AID-NME876>3.0.CO;2-S`.

[19] G. B. Folland. *Fourier analysis and its applications.* The Wadsworth & Brooks/Cole mathematics series. California: Wadsworth & Brooks/Cole Advanced Books & Software, 1992. ISBN: 0534170943.

[20] S. Olsson. Point force excitation of an elastic infinite circular cylinder with an embedded spherical cavity. *J. Acoust. Soc. Am.* **93**.5 (1993), 2479–2488. DOI: `10.1121/1.405869`.

[21] A. Boström and H. Wirdelius. Ultrasonic probe modeling and nondestructive crack detection. *J. Acoust. Soc. Am.* **97**.5 (1995), 2836–2848. DOI: `10.1121/1.411850`.

[22] A. Boström and P. Bövik. Ultrasonic scattering by a side-drilled hole. *Int. J. Solids Struct.* **40**.13–14 (2003), 3493–3505. DOI: `10.1016/S0020-7683(03)00150-1`.

[23] B. A. Auld. General electromechanical reciprocity relations applied to the calculation of elastic wave scattering coefficients. *Wave Motion* **1**.1 (1979), 3–10. DOI: `10.1016/0165-2125(79)90020-9`.